

Learning Event-based Spatio-Temporal Feature Descriptors via Local Synaptic Plasticity: A Biologically-realistic Perspective of Computer Vision

Ali Safa^{1,2}, Hichem Sahli^{2,3}, André Bourdoux², Ilja Ocket^{1,2}, Francky Catthoor^{1,2}, Georges Gielen^{1,2}
¹KU Leuven, ²imec, 3001, Leuven, ³ETRO VUB, 1050, Brussels, Belgium

Ali.Safa@imec.be

Abstract

We present an optimization-based theory describing spiking cortical ensembles equipped with Spike-Timing-Dependent Plasticity (STDP) learning, as empirically observed in the visual cortex. Using our methods, we build a class of fully-connected, convolutional and action-based feature descriptors for event-based camera that we respectively assess on N-MNIST, challenging CIFAR10-DVS and on the IBM DVS128 gesture dataset. We report significant accuracy improvements compared to conventional state-of-the-art event-based feature descriptors (+8% on CIFAR10-DVS). We report large improvements in accuracy compared to state-of-the-art STDP-based systems (+10% on N-MNIST, +7.74% on IBM DVS128 Gesture). In addition to ultra-low-power learning in neuromorphic edge devices, our work helps paving the way towards a biologically-realistic, optimization-based theory of cortical vision.

1. Introduction

This paper provides a theoretical framework for unsupervised feature learning in the visual cortex and applies the introduced theory for object classification and action recognition using event-based cameras. In contrast to deep learning, a biologically-realistic neural learning system must comply with the following characteristics. First, neurons must communicate through action potentials (or spikes) in an event-based, asynchronous manner [34] (vs. frame-based, graded potential activations used in deep learning). Second, learning must be unsupervised and rely on rules that only use local information to each neuron in order to modify the synaptic weights [19] (vs. traditional supervised training and error back-propagation in deep learning). Learning is implemented through Spike-Timing-Dependent Plasticity (STDP) as empirically observed in the brain [5].

Besides its interest as part of a theory of mind, studying biologically-realistic (bio-) neural ensembles will enable a generation of ultra-low-power and -area, neuromorphic vi-

sion systems [44] integrating unsupervised, on-line learning in the sensor chips themselves [7, 11, 23, 30, 44].

On the other hand, event-based cameras have been proposed as novel bio-inspired vision sensors composed of independent pixels $\bar{p}_{i,j}$ that fire events asynchronously whenever the change magnitude in light log-intensity $|\Delta L_{i,j}|$ crosses a threshold C [12]. The events have a positive polarity when $\Delta L_{i,j} > 0$ and vice versa when negative [12]. Their event-based and spiking nature is therefore directly compatible with bio-networks that we investigate in this work [36]. Event-based cameras offers a number of advantages compared to standard imaging shutters such as a fine-grain time resolution ($\sim 1\mu s$), a high dynamic range ($\sim 120\text{dB}$ vs. $\sim 60\text{dB}$ for imaging cameras) and a reduced data communication bandwidth (memory usage) [12]. Those characteristics make event-based cameras well-suited for applications such as drone navigation [10] and IoT [36] where computing must be done at the extreme edge, with the tightest of energy and area budgets (same scope as our bio-neural learning study).

However, spiking neural networks equipped with STDP learning are currently inferior in many aspects compared to conventional methods [41]. For one, they have been demonstrated on a significantly smaller and simpler number of applications, and often reach inferior inference performances compared to conventional methods (e.g., classification accuracy) [30]. Secondly, designing such systems often involves the careful hand-tuning of dozens of hyperparameters (neuron thresholds, time constants, STDP parameters and so on) [13]. Thirdly, it is often unknown what exact optimization objectives those STDP learning systems are solving, adding uncertainty to their design and behaviour [3, 13, 37, 38].

We argue that the main limiting factor for bio-neural ensembles that learn through STDP is the lack of an optimization-based theoretical approach that bridges the gap between conventional pattern learning and the biological evidence. Earlier works shed light on the link between PCA decomposition [21], dictionary learning and *non-spiking* local learning rules (not STDP), often requir-

ing *non-biologically-realistic* components and modulation signals [24]. In this paper, we propose to greatly generalize the theoretical description of STDP-based learning system by explaining them through the framework of joint dictionary learning and basis pursuit (DLBP) via LASSO coding [4]. We derive a number of constraints between the system hyper-parameters and propose an approach based on the corrected Akaike information criterion (AIC_c) [1] for neural parameter tuning, reducing design time.

Finally, we use our framework to build feature descriptors and we assess their performance on three event-based camera datasets for object and action recognition [2,22,27].

2. Related work

2.1. Feature descriptors for event-based cameras

A number of feature descriptors have been proposed for summarizing spatio-temporal information of event data into frame-based vectors that can be subsequently classified by conventional approaches such as support vector machines (SVMs) [18, 20, 31, 36]. Most recent among them, the *Histogram of Averaged Time Surfaces* (HATS) [36] has been proposed as a *hand-crafted* computationally-efficient descriptor formed by concatenating normalized histograms from local patches obtained after a time surface transform of the event data. The *Distribution Aware Retinal Transform* (DART) [31] has been later proposed, which first builds local histograms of events in log-polar grids and then, applies k-means clustering to learn an *under-complete* codebook from the local histograms (used to encode the histograms during inference). DART has been shown to outperform HATS on the challenging CIFAR10-DVS dataset [22]. A similar method has been proposed by *Kostadinov et al.* [18] with the difference that histograms are formed using Cartesian grids and an *over-complete* codebook is learned through conventional K-SVD *dictionary learning* [27].

Compared to the feature descriptors that incorporate learning (i.e., DART [31] and the approach of *Kostadinov et al.* [18]), our method is the only one using a bio-learning rule (STDP as observed in the brain [5]). Compared to the aforementioned works, our method outperforms them in terms of classification accuracy (see Section 6). Our system works directly in the event domain and enables learning in ultra-low-power neuromorphic hardware.

2.2. Bio-networks trained using STDP

A large number of *Spiking Neural Networks* (SNNs) trained through STDP have been proposed in literature and assessed on low-dimensional tasks [38] such as MNIST [8], ECG classification [3] or 2-class image datasets [26]. Their study is important for two main reasons. First, for uncovering the ways through which the human brain learns. Second, to build ultra-low-power learning systems for extreme

edge computing [44]. To the best of our knowledge, the vast majority of previous STDP work share in common the fact that they are designed empirically, following biological observations and heuristics (*bottom-up*), which often involves the fine-tuning of dozens of parameters [25].

In contrast, we adopt a *top-down* approach by first formulating an optimization problem and then, solving it using an SNN equipped with STDP. Our methods take their roots in several works [21, 24, 32, 39] but deviates from them in terms of architectural differences (e.g., use of STDP) and test dataset complexity. Our approach outperforms conventional event-based feature descriptors on several datasets; *significantly* outperforms the most recent STDP-based systems [13, 25] in accuracy; and helps building an optimization-based *theory of cortical vision*.

3. Methods

3.1. Proposed bio-neural topology

Fig. 1 shows our proposed SNN circuit (Fig. 1 a) and details the spiking *units of computation* (UoC) (Fig. 1 b, c). Each UoC is a fully independent entity build around a push-pull pair of LIF neurons, and possesses its own set of weight vectors (synapses) that are learned *locally* via STDP. We consider pairs of neurons (i.e., positive and negative outputs) as it enables the network to perform an approximate LASSO regression (vs. approximating a positively-constrained LASSO as in [24] where only push neurons are used). This is compatible with a bio-approach following empirical evidence about the existence of such pairs in both the motor cortex [14] and within retinal ganglions and lateral geniculate nucleus cells that code light intensities [16]. Each UoC can be implemented as an independent, *systolic* unit in hardware, enabling a massively parallel implementation of the SNN circuit. Next, we show that our SNN-STDP system provably solves the DLBP problem (1,11).

3.2. Basis Pursuit

Let the *LASSO* basis pursuit problem be defined by:

$$\bar{c} = \arg \min_{\bar{c}} \frac{1}{2} \|\Phi \bar{c} - \bar{s}\|_2^2 + \lambda_1 \|\bar{c}\|_1 \quad (1)$$

with Φ a $N \times M$ dictionary featuring M atoms, \bar{s} a N -dimensional input vector, \bar{c} a M -dimensional sparse code and λ_1 a hyper-parameter defining the *support* κ (number of non-zero entries) of \bar{c} (the higher λ_1 , the smaller κ). The global solution to (1) is classically found using the *iterative soft-thresholding algorithm* (ISTA) [6]:

$$\bar{c}^{k+1} = \text{Prox}_{\lambda_1 \|\cdot\|_1} \{ \bar{c}^k - \eta_1 \Phi \Phi^t \bar{c}^k + \eta_1 \Phi \bar{s} \} \quad (2)$$

with η_1 the convergence rate, k the iteration step and

$$\text{Prox}_{\lambda_1 \|\cdot\|_1} \{ \bar{x} \}_i = \text{sign}(x_i) \max(|x_i| - \lambda, 0) \quad (3)$$

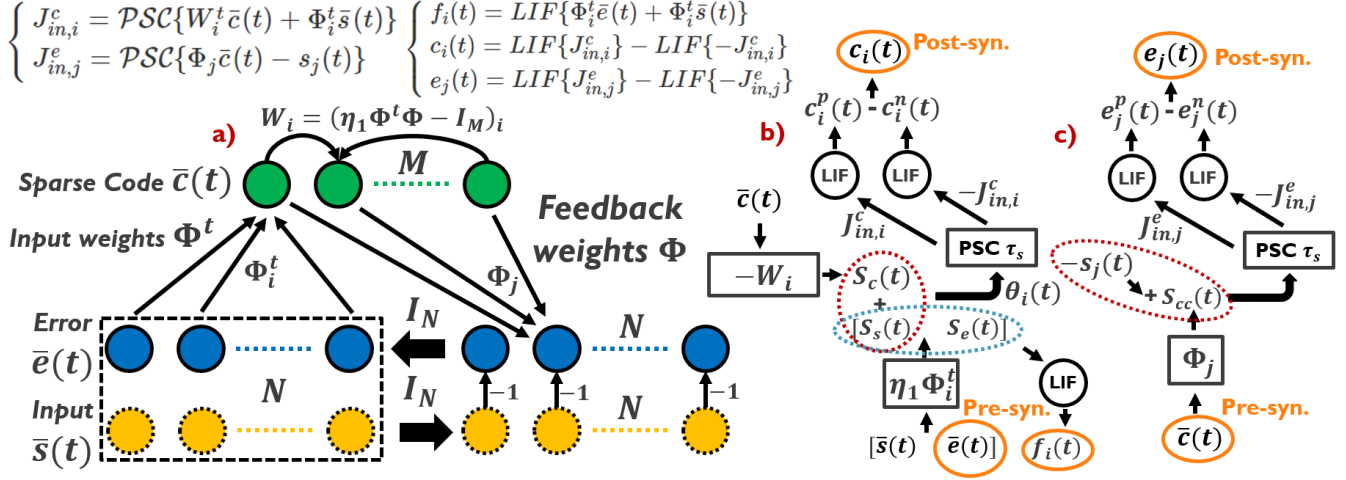


Figure 1. Proposed SNN-STDP circuit for joint dictionary learning and basis pursuit. a) gives a high-level view of the SNN topology. $\bar{s}(t)$ is the input spike train vector of dimension N , I_N is the identity matrix, $\bar{e}(t)$ is the spiking output vector of the error layer (in blue), Φ^t is the $M \times N$ input weight matrix, $\bar{c}(t)$ is the M -dimensional spiking output vector of the coding layer (in green), $W = \eta_1 \Phi^t \Phi - I_M$ is the winner-take-all (WTA) weight matrix and Φ is the feedback weight matrix from the coding layer to the error layer. b) description of the unit of computation (UoC) used in the coding layer. The i^{th} UoC in the coding layer receives the input $\bar{s}(t)$, the error $\bar{e}(t)$ and the sparse code $\bar{c}(t)$ spike train vector (analogous to *pyramidal neurons* in the visual cortex [33]). The single-ended spike trains $\eta_1 \Phi_i^t \bar{s}(t)$ and $W_i \bar{c}(t)$ are superimposed and fed as a single spike train $\theta_i(t)$ to the post-synaptic current (PSC) filter. The resulting signal $J_{in,i}^c(t)$ and its opposite are respectively fed to a push and a pull LIF neuron. The push-pull spiking outputs are then combined as a single-ended spike train $c_i(t) = c_i^p(t) - c_i^n(t)$. STDP learning is applied to Φ_i^t with $\bar{e}(t)$ as the pre-synaptic spike trains and $c_i(t)$ as the post-synaptic spike train (20). STDP is also applied to W_i using (27). c) description of the UoC in the error layer. The j^{th} UoC in the error layer receives $\bar{c}(t)$ and $-s_j(t)$ as input and the signal $J_{in,j}^e(t)$ is obtained as the result of PSC filtering of the spike train $-s_j(t) + \Phi_j \bar{c}(t)$. Similar to the coding UoCs in b), a pair of LIF neurons produce a push-pull spike trains which are combined as $e_j(t) = e_j^p(t) - e_j^n(t)$. STDP learning is applied to Φ_j with $\bar{c}(t)$ as the pre-synaptic spike trains and $e_j(t)$ as the post-synaptic spike train (23).

the proximal operator to the l_1 norm [6]. Unless stated otherwise, we assume Poisson-distributed spike trains throughout this paper (i.e., only the *mean spike rate* bears information). Let \bar{J}_{in}^c the input current vector to neurons defined as $\bar{J}_{in}^c = \mathcal{PSC}\{\bar{\theta}(t)\}$ where $\bar{\theta} = \eta_1 \Phi^t \bar{s} - W \bar{c}$ (see Fig. 1 b) and $\mathcal{PSC}\{\cdot\}$ is the post-synaptic current filter (PSC):

$$\mathcal{PSC}\{\bar{\theta}(t)\} = \bar{\theta}(t) * \frac{1}{\tau_s} e^{-t/\tau_s} \quad (4)$$

where τ_s defines the bandwidth of the PSC kernel (exponential decay) placed at the input of each spiking neuron in our SNN (see Fig. 1 b, c). We define the pair of *leaky integrate and fire* (LIF) neurons [30]:

$$\frac{d}{dt} \begin{bmatrix} V_p^i \\ V_n^i \end{bmatrix} = \frac{1}{\tau_m} \left(\begin{bmatrix} J_{in,i}^c \\ -J_{in,i}^c \end{bmatrix} - \begin{bmatrix} V_p^i \\ V_n^i \end{bmatrix} \right) \quad (5)$$

where V_p^i and V_n^i respectively denote the push and pull membrane potential, τ_m is the membrane time constant and x_i is the input current obtained after filtering a *spiking* input by the PSC kernel (4). As soon as V_p^i or V_n^i exceed a threshold μ , the membrane potential is reset to 0 and the corresponding push or pull output emits a spike:

$$\begin{bmatrix} \sigma_p^i \\ \sigma_n^i \end{bmatrix} = \bar{\mathbb{I}} \left\{ \begin{bmatrix} V_p^i \\ V_n^i \end{bmatrix} \geq \mu \right\} \quad (6)$$

where σ_p^i and σ_n^i respectively denote the push and pull spiking output and $\bar{\mathbb{I}}$ is the indicator function. We refer to the application of the LIF non-linearity (5.6) as $LIF\{\cdot\}$ in the following discussions. Before showing how (5) solves (1), it follows from the LIF rate analysis in [9] that a first-order approximation between the spiking rates of our UoC and the input current x_i is given by:

$$\begin{bmatrix} r_p^i \\ r_n^i \end{bmatrix} \approx \frac{1}{\tau_m \mu} \begin{bmatrix} J_{in,i}^c - \mu \text{ if } J_{in,i}^c > \mu \text{ else } 0 \\ J_{in,i}^c + \mu \text{ if } J_{in,i}^c < -\mu \text{ else } 0 \end{bmatrix} \quad (7)$$

which is equivalent to the proximal operator (3) if:

$$\tau_m = \frac{1}{\mu} \quad (8)$$

in order to have a slope of 1. Therefore, a layer composed of M coding UoCs acts as (3) in the rate-based domain. Following (7) and (8), we can write the effect of the coding layer (green UoCs in Fig. 1 a) of our SNN topology as:

$$\bar{c}^{k+1} = \begin{bmatrix} 1 & 1 \end{bmatrix} \begin{bmatrix} \bar{r}_p \\ \bar{r}_n \end{bmatrix}^{k+1} \approx \text{Prox}_{\mu, \|\cdot\|_1} \{ \bar{J}_{in}^c \} \quad (9)$$

Finally, it follows directly from (2) that wiring the coding UoCs as follows (with $W = \eta_1 \Phi \Phi^t - I$ in Fig. 1):

$$\bar{J}_{in}^c = \mathcal{PSC}\{ \eta_1 \Phi \bar{s}(t) - (\eta_1 \Phi \Phi^t - I) \bar{c}(t) \} \quad (10)$$

as done in the coding layer of our SNN (green UoC layer in Fig. 1 a) makes the SNN iteration steps behave as in (2) which in turn, makes the push-pull output rates converge to the solution of (1).

3.3. Dictionary Learning with STDP

The dictionary learning problem is defined by:

$$\Phi = \arg \min_{\Phi} \frac{1}{2} \|\Phi \bar{c} - \bar{s}\|_2^2 + \frac{\lambda_2}{2} \|\Phi\|_F^2 \quad (11)$$

where λ_2 is a weight decay hyper-parameter (also called *homeostasis* in neuroscience [40]). Eq. (11) is classically solved by iterating as:

$$\Phi^{k+1} = \Phi^k - \eta_2 (\Phi \bar{c} - \bar{s}) \bar{c}^t - \eta_2 \lambda_2 \Phi^k \quad (12)$$

where η_2 is the dictionary learning rate. In the remaining of this section, we show how (11) is solved via STDP using our SNN topology of Fig. 1. Let $\Delta t = t_{post} - t_{pre}$ be the time difference between a post- and a pre-synaptic spike. The synapse is modified according to the double exponential STDP rule empirically observed in the brain [5]:

$$\kappa(\Delta t) = \begin{cases} A_+ e^{-\Delta t / \tau_+}, & \text{if } \Delta t \geq 0 \\ -A_- e^{\Delta t / \tau_-}, & \text{if } \Delta t < 0 \end{cases} \quad (13)$$

where A_+ , A_- are the potentiation and depression weights, and τ_+ , τ_- are the potentiation and depression time constants. Given a pre-synaptic spike train $s_{pre}(t)$ and a post-synaptic spike train $s_{post}(t)$, we can write the weight modification of the synapse at the post-synaptic time instant t as:

$$\Delta w|_t = \eta_2 \int_{-\infty}^{\infty} s_{post}(t) s_{pre}(t - \tau) \kappa(\tau) d\tau \quad (14)$$

Under its current form, (14) is not helpful as the post- and pre-synaptic spike trains cannot be known *a priori*. Taking the expected value of (14), we obtain:

$$\mathcal{E}\{\Delta w|_t\} = \eta_2 \int_{-\infty}^{\infty} \mathcal{E}\{s_{post}(t) s_{pre}(t - \tau)\} \kappa(\tau) d\tau \quad (15)$$

which can be written as:

$$\mathcal{E}\{\Delta w|_t\} = \eta_2 \int_{-\infty}^{\infty} \{r_{post} r_{pre} + \mathcal{C}(\tau)\} \kappa(\tau) d\tau \quad (16)$$

where r_{post} , r_{pre} are the post- and pre-synaptic spike rates, and $\mathcal{C}(\tau)$ is the covariance between the pre- and post-synaptic spike train. Eq. (16) can be further separated into a rate-based term and a covariance term:

$$\begin{aligned} \mathcal{E}\{\Delta w|_t\} &= \eta_2 (A_+ \tau_+ - A_- \tau_-) r_{post} r_{pre} \\ &+ \eta_2 \int_{-\infty}^{\infty} \mathcal{C}(\tau) \kappa(\tau) d\tau \end{aligned} \quad (17)$$

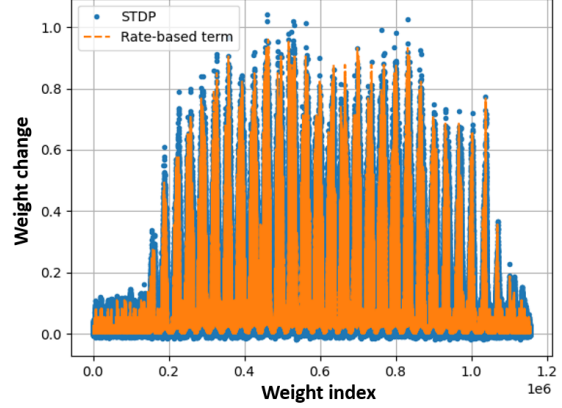


Figure 2. STDP weight change vs. rate-based term (18) obtained by recording the accumulated synaptic change of the input weights to the coding layer Φ during 300 time-steps with the N-MNIST dataset [27]. The prediction error made by the rate-based model is $\frac{1}{MN} \sum_{i=1}^{MN} |\Delta w_{STDP}^i - \Delta w_{rate}^i| \approx 2 \times 10^{-5}$

In order to evaluate the impact that each term has on synaptic plasticity, we compare in Fig. 2 the experimental weight change induced by STDP Δw_{STDP} to the weight change Δw_{rate} that would be induced by the rate-based term of (17) only. Fig. 2 clearly shows that the *long-term* STDP weight change is well explained by the rate-based term of (17). Therefore, in the rest of our derivation, we approximate:

$$\Delta w_{STDP}\{s_{post}, s_{pre}\} \approx \eta_2 (A_+ \tau_+ - A_- \tau_-) r_{post} r_{pre} \quad (18)$$

where we assume, without loss of generality, that:

$$A_+ \tau_+ - A_- \tau_- = 1 \quad (19)$$

such that the resulting learning rate is not modified (ensuring $A_+ \tau_+ - A_- \tau_- > 0$ is enough for the learning to take place). Under the light of (18), we can now show how the dictionary is learned in each set of weights (input weights, feedback weights and WTA weights).

3.3.1 Input weights

Each *coding* UoC possesses one row i of the input weight matrix Φ^t that we note Φ_i^t . By modifying each element j of Φ_i^t using the local STDP update rule with regularisation:

$$(\Phi_i^t)_j \leftarrow (\Phi_i^t)_j - \Delta w_{STDP}\{c_i(t), e_j(t)\} - \eta_2 \lambda_2 (\Phi_i^t)_j \quad (20)$$

and by using (18) and (19), (20) can be written as:

$$(\Phi_i^t)_j \leftarrow (\Phi_i^t)_j - \eta_2 \mathcal{PSC}\{c_i(t)\} \mathcal{PSC}\{e_j(t)\} - \eta_2 \lambda_2 (\Phi_i^t)_j \quad (21)$$

where the PSC filters estimate the spiking rates r_{post} , r_{pre} . As our SNN topology in Fig. 1 a) ensures:

$$e_j = \Phi_j \bar{c} - s_j \quad (22)$$

it is now clear that, under the STDP rate-based approximation (18), (20) is indeed solving (12).

3.3.2 Feedback weights

Each *error* UoC (blue units in Fig. 1 a) possesses one row j of the input weight matrix Φ that we note Φ_j . By modifying each element i of Φ_j using the local STDP update rule with homeostasis regularisation:

$$(\Phi_j)_i \leftarrow (\Phi_j)_i - \Delta w_{\text{STDP}}\{e_j(t), c_i(t)\} - \eta_2 \lambda_2 (\Phi_j)_i \quad (23)$$

it directly follows from the discussion on input weights (section 3.3.1) that (23) solves (12) for the error layer.

3.3.3 WTA weights

To learn the WTA weights W , we adapt the *consistency-enforcing* strategy:

$$\tilde{W} = \arg \min_{\tilde{W}} \frac{1}{2} \|(\tilde{W} - \Phi^t \Phi) \bar{c}\|_2^2 \quad (24)$$

proposed in [24] to our use of the STDP rule, where $W = \eta_1 \tilde{W} - I_M$. Eq. (24) is classically solved by iterating:

$$\tilde{W}^{k+1} = \tilde{W}^k - (\tilde{W}^k - \Phi^t \Phi) \bar{c} \bar{c}^t \quad (25)$$

In each *coding* UoC i , only the i^{th} row of W and Φ^t are available. In addition, the spike train vectors $\bar{S}(t)$, $\bar{c}(t)$ and $\bar{e}(t)$ are available as well. The single-ended spike train $f_i(t)$, representing $(\tilde{W} - \Phi^t \Phi)_i \bar{c}$ through the rate $\mathcal{PSC}\{f_i(t)\}$, is computed as the internal spiking state:

$$\begin{aligned} f_i(t) &= \text{LIF} \left\{ \frac{1}{\eta_1} (W + I_M)_i \bar{c}(t) - (\Phi^t)_i \bar{e}(t) + (\Phi^t)_i \bar{s}(t) \right\} \\ &= \text{LIF} \{ (\tilde{W} - \Phi^t \Phi)_i \bar{c}(t) \} \end{aligned} \quad (26)$$

since $\bar{e}(t) + \bar{s}(t) = \Phi \bar{c}(t)$ in Fig. 1. It is then clear that the STDP update (where $i = 1, \dots, M$ spans the rows and $l = 1, \dots, M$ spans the columns of \tilde{W}):

$$(\tilde{W}_i)_l \leftarrow (\tilde{W}_i)_l - \Delta w_{\text{STDP}}\{f_i(t), c_l(t)\} - \eta_2 \lambda_2 (\tilde{W}_i)_l \quad (27)$$

solves (24, 25). At this point, we have shown that, under the rate-based approximation, our proposed SNN system jointly solves the dictionary learning (11) and the basis pursuit (1) problems. Still, three questions remain. How to tune the parameters of the STDP rule (13)? How to initialize the network weights? How to optimally tune the LIF neuron threshold μ and time constant τ_m in (5, 6)?

4. Parameter study

4.1. STDP parameter tuning

Eq. (14) clearly shows that the STDP kernel $\kappa(\tau)$ filters $s_{pre}(t)$ over a certain bandwidth $B\{A_+, A_-, \tau_+, \tau_-\}$.

Therefore, we must insure that the pass-band is matching the useful spectrum of $s_{pre}(t)$ while filtering noise and the spurious frequencies due to the distortion (caused by the discontinuous nature of spike trains). Taking the Fourier transform of (13):

$$\mathcal{F}\{\kappa(t)\} = \frac{A_+}{\tau_+^{-1} + j\omega} - \frac{A_-}{\tau_-^{-1} - j\omega} \quad (28)$$

The spectral magnitude of (28) is then given by:

$$|\mathcal{F}\{\kappa(t)\}| = \frac{A_+ \sqrt{(\tau_-^{-1} - \alpha \tau_+^{-1})^2 + (1 + \alpha)^2 \omega^2}}{\sqrt{\tau_+^2 + \omega^2} \sqrt{\tau_-^2 + \omega^2}} \quad (29)$$

where $\alpha = A_-/A_+$. Analysing (29), we identify two poles $\omega_{1,2}$ and one zero z_1 :

$$\omega_1 = \tau_+^{-1} \quad \omega_2 = \tau_-^{-1} \quad z_1 = \frac{\tau_-^{-1} - \alpha \tau_+^{-1}}{1 + \alpha} \quad (30)$$

Eq. (14, 30) show that STDP acts as a first-order bandpass filter on $s_{pre}(t)$. As we have assumed Poisson-distributed spike trains throughout this work, the *useful information* carried by a spike train $s(t)$ is its spiking rate and therefore, solely resides in the DC bin $\mathcal{F}\{s(t)\}|_{\omega=0}$ (all other bins containing noise and distortion under the Poisson assumption). As such, the spectrum of the STDP kernel must avoid cutting the DC frequency while attenuating AC bins in order to match the information band of the Poisson spike trains. Regarding real-world event-based camera data, the Poisson assumption does not hold anymore but rather, the spike train bandwidth covers a narrow information band around DC as shown in Fig. 3 and a similar discussion holds (i.e., STDP must not cut around DC). A nearly flat STDP spectrum around DC is obtained by pole-zero cancellation of ω_1 and z_1 in (29), (30). This leads to the constraint:

$$\tau_+^{-1} = \frac{\tau_-^{-1} - \alpha \tau_+^{-1}}{1 + \alpha} \quad (31)$$

Fig. 3 shows a matching STDP spectrum which complies with (31). In contrast, the non-matching STDP spectrum in Fig. 3 strongly attenuates the information-bearing frequency band, while passing noise. A non-matching STDP kernel will thus result in the learning of noisier atoms Φ_i compared to a matching STDP kernel, degrading the quality of the learned dictionary (see Section A in supplementary material for experimental demonstrations).

4.2. Weight initialisation

The weight matrix Φ is randomly initialized following a zero-mean Gaussian distribution with standard deviation σ $\Phi \sim \mathcal{N}(0, \sigma)$. Setting $\lambda_1 = 0$ and $\eta_1 = 1$ in (2), it follows:

$$\bar{c}^k = (I_M - \Phi \Phi^t)^k \bar{c}^0 + \sum_{p=0}^{k-1} (I_M - \Phi \Phi^t)^p \Phi \bar{s} \quad (32)$$

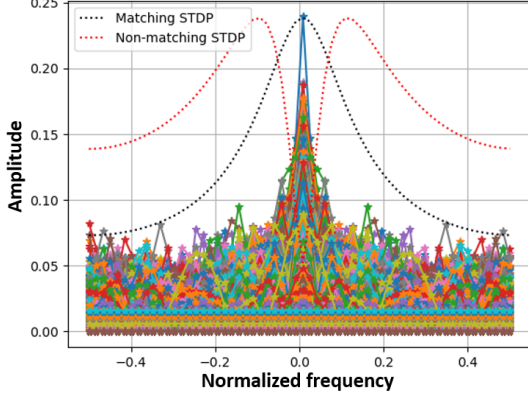


Figure 3. Real-world event-based camera spectra acquired by applying the DFT (with a Hanning window to reduce spectral leakage) on each pixel spike train from N-MNIST acquisitions [27]. The matching STDP kernel is tuned via ω_2 such that its -3dB point covers the useful part of the spectrum, with the STDP parameters $A_+ = 1, A_- = 0.8, \tau_+ = 0.0208\text{s}, \tau_- = 0.008\text{s}$. In contrast, the non-matching STDP kernel ($A_+ = 1, A_- = 0.8, \tau_+ = 0.008\text{s}, \tau_- = 0.008\text{s}$) does not comply with (31) and degrades the useful part of the spectrum.

which converges if the *spectral radius* of $(I_M - \Phi\Phi^t)$ is smaller than unity. It follows directly that:

$$|1 - M\sigma^2| < 1 \Rightarrow \sigma < \sqrt{\frac{2}{M}} \quad (33)$$

The weight initialization condition (33) naturally holds in the case where $\lambda_1 > 0$ in (2) since the l_1 norm in (1) *shrinks* the entries of \bar{c}^k throughout the iterations, leading to a more stable process compared to (32).

4.3. Neural parameter tuning

A typical problem faced when designing SNN-STDP learning systems is the choice of the neuron threshold μ and the membrane time constant τ_m . Those parameters are often identified via *brute force* procedures such as manual search or automated grid search, iterating between training the whole system (SNN and eg., SVM classifier) with the updated parameters and testing the resulting model. Clearly, such approach is too time- and power-consuming, making it ill-suited for latency- and cost-sensitive *edge learning*. In contrast, we first use the derived proximal constraint (8) to reduce the problem to a one-dimensional search along μ only. Secondly, we avoid retraining and iterative testing of the learning system (SNN and readout classifier) during the pursuit of μ by exploiting the activity of the error layer in our SNN topology (blue UoCs in Fig. 1) within a *maximum a posteriori*, Akaike-based approach. The AIC_c is defined as follows [1]:

$$AIC_c = -2 \ln \mathcal{P}_{\kappa(\mu)}(\bar{S}_l, \Phi) + 2\kappa(\mu) + \frac{2\kappa^2 + 2\kappa}{N - \kappa - 1} \quad (34)$$

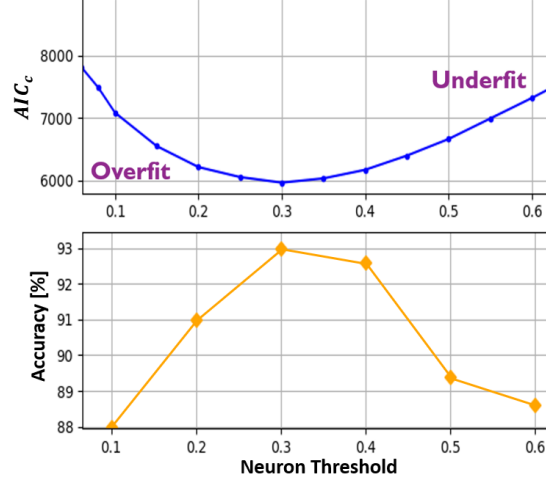


Figure 4. Relation between the corrected AIC (34) and linear SVM classification accuracy. Generated using $M = 100$ coding neurons. Assessed on N-MNIST [27]. The overfit region corresponds to the case where the neuron threshold μ is too small, leading to a large number of non-zero coefficients (and vice versa).

where \bar{S}_l is an input vector from the dataset, Φ is the model parameter matrix (weights), $\mathcal{P}_{\kappa(\mu)}(\bar{S}, \Phi)$ is a likelihood hypothesis, N is the input dimension and $\kappa(\mu)$ is the number of non-zero elements of the output spike rate vector $\mathcal{PSC}(\bar{c})$ (the higher the neuron threshold μ , the smaller the κ). As a likelihood hypothesis in the spike rate domain, we choose the typical Gaussian model [1]:

$$\mathcal{P}_{\kappa(\mu)}(\bar{S}_l, \Phi) \sim \exp - \frac{1}{2} \frac{\|\mathcal{PSC}\{\bar{e}_l(t)\}\|_2^2}{\sigma_z^2} \quad (35)$$

where $\mathcal{PSC}\{\bar{e}_l(t)\}$ is the re-projection error in the *spike-rate* domain (or the *inner loss* of the model). In practice, we evaluate this likelihood over a small number of training examples $N_{\text{mini}} \sim 10$. The *maximum likelihood* estimate (MLE) of the error spike-rate noise variance σ_z^2 is evaluated as the variance of $\mathcal{PSC}\{\bar{e}_l\}$, $\forall l \in N_{\text{mini}}$ in the limit $\mu \rightarrow 0$ (corresponding to $\lambda_1 \rightarrow 0$), reducing (1) to the *ordinary least-squares* (OLS) fitting problem. In practice, we define an array of μ values to test in ascending order and we estimate σ_z^2 during the first iteration of our Akaike-based pursuit (smallest μ within the values to test). Fig. 4 shows the relation between AIC_c and the accuracy of the classification system obtained by using a linear SVM. As expected, the minimum-AIC threshold $\hat{\mu}$ gives a good indication of the region where an accuracy-maximising μ can be found.

5. Building feature descriptors

5.1. Fully-connected descriptor

We use our SNN-STDP framework to learn fully-connected feature descriptors by flattening the event-based

camera images and feeding them as spiking vectors to the SNN. A question rarely addressed in prior STDP-based works is the number of epochs needed before stopping the learning process, due to the unavailability of a loss function used to cross-validate the fitting performance of the SNN-STDP system. In contrast, our SNN-STDP topology features an error layer (blue UoCs in Fig. 1) with an associated *inner loss* $\|\mathcal{PSC}\{\bar{e}(t)\}\|_2^2$. Therefore, a small validation set can be extracted from the training set and periodically used to assess the reprojection quality of the model during training (see Section B in supplementary material for an illustration). Learning is stopped when the inner loss on the validation set hits a plateau. A feature descriptor $\bar{\mathcal{F}}_{fc}$ containing the mean rate of each spiking output $\mathcal{PSC}\{\bar{c}(t)\}$ is obtained during inference and normalized to unit norm to provide invariance to event density:

$$\bar{\mathcal{F}}_{fc} = \frac{\mathcal{PSC}\{\bar{c}(t)\}}{\|\mathcal{PSC}\{\bar{c}(t)\}\|_2} \quad (36)$$

5.2. Action descriptor

The fully-connected descriptor of Section 5.1 can be extended for recognising macro-actions such as gestures performed in front of an event-based camera. In contrast to *saccades* (event-based camera vibration used to acquire e.g., N-MNIST images [27]), macro-actions result in enhanced spiking rate oscillations at the output of our SNN-STDP system due to the periodicity in gestures (e.g., a hand rotation). To capture correlations between the oscillating spiking rates, we concatenate (noted \oplus) the Pearson correlation matrix of $\mathcal{PSC}\{\bar{c}(t)\}$ noted ρ (the correlation being computed along the time domain, capturing changes in spike rate), with the outer product matrix of the output mean rate vectors $P = \mathcal{PSC}\{\bar{c}(t)\}\mathcal{PSC}\{\bar{c}(t)\}^T$ as follows:

$$\bar{\mathcal{F}}_{ac} = \frac{\rho_{tri} \oplus P_{tri}}{\|\rho_{tri} \oplus P_{tri}\|_2} \quad (37)$$

where the *tri* denotes the upper triangular part of the matrix.

5.3. Convolutional descriptor

The theoretical framework detailed in Section 3 can naturally be extended to the case of learning convolutional filter banks for capturing translational invariances [28]:

$$\bar{c}, \Phi = \arg \min_{\bar{c}, \Phi} \frac{1}{2} \|\Phi * \bar{c} - \bar{s}\|_2^2 + \lambda_1 \|\bar{c}\|_1 + \frac{\lambda_2}{2} \|\Phi\|_F^2 \quad (38)$$

by sweeping with stride d the $h \times w$ visual field of our SNN-STDP system across the event-camera plane (processed in parallel on GPU in our experiments).

The Akaike-based pursuit of Section 4.3 can then be applied to estimate $\hat{\mu}$. By applying the convolutional SNN-STDP bank of M filters to a $H \times W$ image, a spike-rate tensor $\mathcal{T}_{x,y,c}$ of dimension $l_H \times l_W \times M$ is obtained

($l_H = (H-h)/d+1$ and $l_W = (W-w)/d+1$). The tensor $\mathcal{T}_{x,y,c}$ is then max-pooled at multiple scales a_i using spatial pyramidal pooling (SPP) [15] in order to capture multi-scale features (Fig. C.6 in **supp. mat.**). Doing so, a bag of tensors $\{\mathcal{T}_{x,y,c}^{a_1}, \mathcal{T}_{x,y,c}^{a_2}, \dots\}$ is obtained. Finally, normalization must be done along the filter bank channels $c = 1, \dots, M$ in order to provide invariance to event density. Inspired by [31], we consider the activity along the filter bank dimension c for each pixel (x, y) to represent a histogram of features captured by the SNN-STDP system. Therefore, we normalize the histograms to probability density functions as:

$$\mathcal{T}_{x,y,c}^{a_i} = \frac{|\mathcal{T}_{x,y,c}^{a_i}|}{\sum_c |\mathcal{T}_{x,y,c}^{a_i}|} \forall x, y \quad (39)$$

Finally, the resulting feature vector $\bar{\mathcal{F}}_{cv}$ is obtained by flattening each normalized tensor $\mathcal{T}_{x,y,c}^{a_i} \forall i$ and concatenating the flattened tensors side-by-side.

6. Experimental results

In this section, we assess the performance of our proposed SNN-STDP theory and bio-feature descriptors of Section 5. Similar to previous works, we consistently use standard scaling followed by a linear SVM classifier [29] to evaluate linear separability in the output space (see Sections C and D of supplementary materials for a discussion on *system limitations* and for visualizing learned dictionaries).

6.1. N-MNIST classification

The N-MNIST dataset [27] features standard MNIST images, re-captured using a real-world DVS camera. Each acquisition contains a tensor of spike trains (along time and image space). In order to feed the DVS data to our SNN, the spiking matrices are flattened to 1-dimensional vectors of spike trains (noted $\bar{s}(t)$ in Fig. 1). As the N-MNIST matrices are of dimension 34×34 , the input dimension is $N = 1156$. We use $M = 4000$ coding neurons. The SNN-STDP dictionary is learned by using the first 40 training examples of each class, leading to only $N_{ex} = 400$ training examples in total (see Fig. 5). After the Akaike-based pursuit of $\hat{\mu}$ (defining λ_1), we fit a linear SVM classifier on the complete training set of SNN-encoded DVS examples. We assess the accuracy of our system on the provided test set. Table 1 reports the training parameters. Table 2 reports a superior N-MNIST accuracy for our system compared to state-of-the-art DVS feature descriptors.

η_1	η_2	λ_2	A_+	A_-	τ_+ [s]	τ_- [s]
1	0.003	0.002	1	0.8	0.0208	0.008

Table 1. Learning parameters. The simulation time-step is 0.005s.

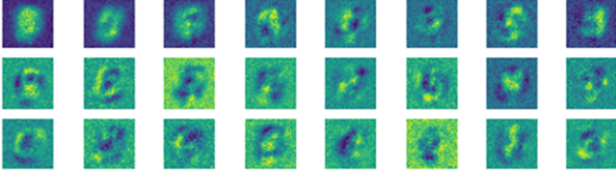


Figure 5. N-MNIST dictionary subset learned by STDP.

Architecture	N-MNIST %	CIFAR10-DVS
MuST (STDP) [25]	89.96	-
HATS [36]	99.1	52.4
DART [31]	97.95	65.78
Kostadinov et al. [18]	98.1	-
Ours (STDP)	99.26	73.98 ± 0.8

Table 2. N-MNIST and CIFAR10-DVS performance. On N-MNIST, our proposed system is the top performer, with close to 10% gain vs. the state-of-the-art STDP system termed MuST [25]. On CIFAR10-DVS, our system outperforms DART by more than 8% and even a deep STS-ResNet [35] (backprop) by close to 4%.

Architecture	IBM DVS128
Reservoir (STDP) [13]	65
SNN-SBP-STDP [45]	84.76
Ours (STDP)	92.5
LSTM [42]	88.17
CNN [2]	91.77
PointNet++ [42]	96.34
STS-ResNet [35]	96.7
CNN-SRNN [43]	97.91

Table 3. 11-class IBM DVS128 performance. Our SNN-STDP system outperforms by 27.5% the state-of-the-art pure STDP-based system proposed in [13] and by 7.74% the STDP-backprop system of [45]. In [13], the authors argue that a source of inefficiency in their system is the fact that STDP training leads to a significant number of noisy, feature-less neurons. In contrast, we did not observe such effect using our proposed SNN-STDP theory. Even though at the advantage of deep learning system (bottom of table), our shallow 1-hidden-layer descriptor outperforms the deep 16-layer CNN of [2] by 0.73%, the LSTM of [42] by 2.5% and achieves an accuracy within 5.41% of the state-of-the-art deep CNN-SRNN of [43] trained through backprop. This is remarkable given the drastically smaller size of our system and its ability for ultra-low-power learning in neuromorphic edge devices.

6.2. CIFAR10-DVS classification

The CIFAR10-DVS dataset [22] features 10000 standard CIFAR10 images (1000 per class) re-captured using a real-world DVS camera at a resolution of 128×128 . We use our proposed SNN-STDP system in the convolutional setting

described in Section 5.3 with a 20×20 visual field ($h = w = 20$), a stride $d = 10$ and $M = 256$ coding neurons (found empirically). We use the same learning parameter as in Table 1. For the SPP layer at the output of the SNN (see Section 5.3), we use a collection of (2×2) , (3×3) , (6×6) and (12×12) max-pooling layers. We train the SNN-STDP system using the first 50 training examples of each class to learn a filter bank capturing features such as edges, corners and so on. After the *a posteriori* estimation of $\hat{\mu}$ using our Akaike-based pursuit, we follow the standard methodology in [31] where we randomly keep 90% of the dataset as the training set and 10% for testing. We repeat this process 10 times with different dataset samplings and report the mean accuracy and standard deviation in Table 2 (+8% vs. [31]).

6.3. IBM DVS128 Gesture classification

Traditionally, event-based feature descriptors have been mostly assessed for image recognition tasks, and less so for action recognition, which has been mostly tackled by end-to-end deep learning systems (see Table 3, [13, 45] being notable exceptions). We argue that it is equally important to assess spatio-temporal descriptors on tasks such as gesture recognition, which better corresponds to real-world applications of event cameras compared to datasets capturing still images with vibrating cameras (see [17] for a comprehensive discussion). To this end, we assess our system as an action descriptor (see Section 5.2) with $M = 1500$ coding neurons on the IBM DVS128 gesture dataset [2] following the train-test procedure of [2]. We outperform same-class methods (+7.74%) and even two deep networks in Table 3.

7. Conclusion

In this work, we have proposed a comprehensive, optimization-based theory describing how biologically-realistic SNNs using STDP learning can perform unsupervised feature extraction. We have applied our proposed method on different event-based camera datasets. We have reported several accuracy improvements over the state of the art (+8% on CIFAR10-DVS compared to conventional descriptors, +10% on N-MNIST and +7.74% on IBM DVS128 Gesture compared to state-of-the-art STDP systems) which adds to the significance of our methods given the small size of our network, its ability for ultra-low-power learning in neuromorphic devices and its bio-realism. To the best of our knowledge, this work will greatly help bridging gaps between computer vision and the human brain.

Acknowledgment

This research received funding from the Flemish Government under the ‘‘Onderzoeksprogramma Artificiële Intelligentie (AI) Vlaanderen’’ programme. The authors thank Dr. Lars Keuninckx for the helpful discussions.

References

- [1] H. Akaike. A new look at the statistical model identification. *IEEE Transactions on Automatic Control*, 19(6):716–723, 1974. [2](#), [6](#)
- [2] Arnon Amir, Brian Taba, David Berg, Timothy Melano, Jeffrey McKinstry, Carmelo Di Nolfo, Tapan Nayak, Alexander Andreopoulos, Guillaume Garreau, Marcela Mendoza, Jeff Kusnitz, Michael Debole, Steve Esser, Tobi Delbruck, Myron Flickner, and Dharmendra Modha. A low power, fully event-based gesture recognition system. In *2017 IEEE Conference on Computer Vision and Pattern Recognition (CVPR)*, pages 7388–7397, 2017. [2](#), [8](#)
- [3] Alireza Amirshahi and Matin Hashemi. Ecg classification algorithm based on stdp and r-stdp neural networks for real-time monitoring on ultra low-power personal wearable devices. *IEEE Transactions on Biomedical Circuits and Systems*, 13(6):1483–1493, 2019. [1](#), [2](#)
- [4] Chenglong Bao, Hui Ji, Yuhui Quan, and Zuowei Shen. Dictionary learning for sparse coding: Algorithms and convergence analysis. *IEEE Transactions on Pattern Analysis and Machine Intelligence*, 38(7):1356–1369, 2016. [2](#)
- [5] Guo-qiang Bi and Mu-ming Poo. Synaptic modifications in cultured hippocampal neurons: Dependence on spike timing, synaptic strength, and postsynaptic cell type. *Journal of Neuroscience*, 18(24):10464–10472, 1998. [1](#), [2](#), [4](#)
- [6] I. Daubechies, M. DeFrise, and C. De Mol. An iterative thresholding algorithm for linear inverse problems with a sparsity constraint. *Communications on Pure and Applied Mathematics*, 57(11):1413–1457, 2004. [2](#), [3](#)
- [7] Mike Davies, Narayan Srinivasa, Tsung-Han Lin, Gautham China, Yongqiang Cao, Sri Harsha Choday, Georgios Dimou, Prasad Joshi, Nabil Imam, Shweta Jain, Yuyun Liao, Chit-Kwan Lin, Andrew Lines, Ruokun Liu, Deepak Mathaikutty, Steven McCoy, Arnab Paul, Jonathan Tse, Guruguhathan Venkataramanan, Yi-Hsin Weng, Andreas Wild, Yoonseok Yang, and Hong Wang. Loihi: A neuromorphic manycore processor with on-chip learning. *IEEE Micro*, 38(1):82–99, 2018. [1](#)
- [8] Peter Diehl and Matthew Cook. Unsupervised learning of digit recognition using spike-timing-dependent plasticity. *Frontiers in Computational Neuroscience*, 9:99, 2015. [2](#)
- [9] Chris Eliasmith and Charles Anderson. *Neural Engineering: Computation, Representation and Dynamics in Neurobiological Systems*. 01 2003. [3](#)
- [10] Davide Falanga, Kevin Kleber, and Davide Scaramuzza. Dynamic obstacle avoidance for quadrotors with event cameras. *Science Robotics*, 5(40):eaaz9712, 2020. [1](#)
- [11] Charlotte Frenkel, Martin Lefebvre, Jean-Didier Legat, and David Bol. A 0.086-mm² 12.7-pj/sop 64k-synapse 256-neuron online-learning digital spiking neuromorphic processor in 28-nm cmos. *IEEE Transactions on Biomedical Circuits and Systems*, 13(1):145–158, 2019. [1](#)
- [12] Guillermo Gallego, Tobi Delbruck, Garrick Michael Orchard, Chiara Bartolozzi, Brian Taba, Andrea Censi, Stefan Leutenegger, Andrew Davison, Jorg Conradt, Kostas Daniilidis, and Davide Scaramuzza. Event-based vision: A survey. *IEEE Transactions on Pattern Analysis and Machine Intelligence*, pages 1–1, 2020. [1](#)
- [13] Arun M. George, Dighanchal Banerjee, Sounak Dey, Arijit Mukherjee, and P. Balamurali. A reservoir-based convolutional spiking neural network for gesture recognition from dvs input. In *2020 International Joint Conference on Neural Networks (IJCNN)*, pages 1–9, 2020. [1](#), [2](#), [8](#)
- [14] Apostolos P. Georgopoulos, Masato Taira, and Alexander Lukashin. Cognitive neurophysiology of the motor cortex. *Science*, 260(5104):47–52, 1993. [2](#)
- [15] Kaiming He, Xiangyu Zhang, Shaoqing Ren, and Jian Sun. Spatial pyramid pooling in deep convolutional networks for visual recognition. *IEEE Transactions on Pattern Analysis and Machine Intelligence*, 37(9):1904–1916, 2015. [7](#)
- [16] D. H. Hubel and T. N. Wiesel. Receptive fields, binocular interaction and functional architecture in the cat’s visual cortex. *The Journal of Physiology*, 160(1):106–154, 1962. [2](#)
- [17] Laxmi R. Iyer, Yansong Chua, and Haizhou Li. Is neuromorphic MNIST neuromorphic? analyzing the discriminative power of neuromorphic datasets in the time domain. *CoRR*, abs/1807.01013, 2018. [8](#)
- [18] Dimche Kostadinov and Davide Scaramuzza. Unsupervised feature learning for event data: Direct vs inverse problem formulation. In *2020 25th International Conference on Pattern Recognition (ICPR)*, pages 5981–5987, 2021. [2](#), [8](#)
- [19] Dmitry Krotov and John J. Hopfield. Unsupervised learning by competing hidden units. *Proceedings of the National Academy of Sciences*, 116(16):7723–7731, 2019. [1](#)
- [20] Xavier Lagorce, Garrick Orchard, Francesco Galluppi, Bertram E. Shi, and Ryad B. Benosman. Hots: A hierarchy of event-based time-surfaces for pattern recognition. *IEEE Transactions on Pattern Analysis and Machine Intelligence*, 39(7):1346–1359, 2017. [2](#)
- [21] Yun-Parn Lee. Multidimensional hebbian learning with temporal coding in neocognitron visual recognition. *IEEE Transactions on Systems, Man, and Cybernetics: Systems*, 47(12):3386–3396, 2017. [1](#), [2](#)
- [22] Hongmin Li, Hanchao Liu, Xiangyang Ji, Guoqi Li, and Luping Shi. Cifar10-dvs: An event-stream dataset for object classification. *Frontiers in Neuroscience*, 11:309, 2017. [2](#), [8](#)
- [23] Qianli Liao, Joel Z. Leibo, and Tomaso Poggio. How important is weight symmetry in backpropagation? In *Proceedings of the Thirtieth AAAI Conference on Artificial Intelligence*, AAAI’16, page 1837–1844. AAAI Press, 2016. [1](#)
- [24] Tsung-Han Lin and Ping Tak Peter Tang. Sparse dictionary learning by dynamical neural networks. In *International Conference on Learning Representations*, 2019. [2](#), [5](#)
- [25] Qianhui Liu, Gang Pan, Haibo Ruan, Dong Xing, Qi Xu, and Huajin Tang. Unsupervised aer object recognition based on multiscale spatio-temporal features and spiking neurons. *IEEE Transactions on Neural Networks and Learning Systems*, 31(12):5300–5311, 2020. [2](#), [8](#)
- [26] Timothée Masquelier and Simon J Thorpe. Unsupervised learning of visual features through spike timing dependent plasticity. *PLOS Computational Biology*, 3(2):1–11, 02 2007. [2](#)

- [27] Garrick Orchard, Ajinkya Jayawant, Gregory K. Cohen, and Nitish Thakor. Converting static image datasets to spiking neuromorphic datasets using saccades. *Frontiers in Neuroscience*, 9:437, 2015. 2, 4, 6, 7
- [28] Vardan Papyan, Yaniv Romano, Michael Elad, and Jeremias Sulam. Convolutional dictionary learning via local processing. In *2017 IEEE International Conference on Computer Vision (ICCV)*, pages 5306–5314, 2017. 7
- [29] Fabian Pedregosa, Gaël Varoquaux, Alexandre Gramfort, Vincent Michel, Bertrand Thirion, Olivier Grisel, Mathieu Blondel, Peter Prettenhofer, Ron Weiss, Vincent Dubourg, Jake Vanderplas, Alexandre Passos, David Cournapeau, Matthieu Brucher, Matthieu Perrot, and Édouard Duchesnay. Scikit-learn: Machine learning in python. *Journal of Machine Learning Research*, 12(85):2825–2830, 2011. 7
- [30] Bipin Rajendran, Abu Sebastian, Michael Schmuker, Narayan Srinivasa, and Evangelos Eleftheriou. Low-power neuromorphic hardware for signal processing applications: A review of architectural and system-level design approaches. *IEEE Signal Processing Magazine*, 36(6):97–110, 2019. 1, 3
- [31] Bharath Ramesh, Hong Yang, Garrick Orchard, Ngoc Anh Le Thi, Shihao Zhang, and Cheng Xiang. Dart: Distribution aware retinal transform for event-based cameras. *IEEE Transactions on Pattern Analysis and Machine Intelligence*, 42(11):2767–2780, 2020. 2, 7, 8
- [32] Christopher Rozell, Don Johnson, Richard Baraniuk, and Bruno Olshausen. Sparse coding via thresholding and local competition in neural circuits. *Neural computation*, 20:2526–63, 05 2008. 2
- [33] João Sacramento, Rui Ponte Costa, Yoshua Bengio, and Walter Senn. Dendritic cortical microcircuits approximate the backpropagation algorithm. In S. Bengio, H. Wallach, H. Larochelle, K. Grauman, N. Cesa-Bianchi, and R. Garnett, editors, *Advances in Neural Information Processing Systems*, volume 31. Curran Associates, Inc., 2018. 3
- [34] Ali Safa, Federico Corradi, Lars Keuninckx, Ilja Ocket, André Bourdoux, Francky Catthoor, and Georges G. E. Gielen. Improving the accuracy of spiking neural networks for radar gesture recognition through preprocessing. *IEEE Transactions on Neural Networks and Learning Systems*, pages 1–13, 2021. 1
- [35] Ali Samadzadeh, Fatemeh Sadat Tabatabaei Far, Ali Javadi, Ahmad Nickabadi, and Morteza Haghiri Chehreghani. Convolutional spiking neural networks for spatio-temporal feature extraction. *CoRR*, abs/2003.12346, 2020. 8
- [36] Amos Sironi, Manuele Brambilla, Nicolas Bourdis, Xavier Lagorce, and Ryad Benosman. Hats: Histograms of averaged time surfaces for robust event-based object classification. In *2018 IEEE/CVF Conference on Computer Vision and Pattern Recognition*, pages 1731–1740, 2018. 1, 2, 8
- [37] Gopalakrishnan Srinivasan, Chankyu Lee, Abhronil Sen Gupta, Priyadarshini Panda, Syed Shakib Sarwar, and Kaushik Roy. Training deep spiking neural networks for energy-efficient neuromorphic computing. In *ICASSP 2020 - 2020 IEEE International Conference on Acoustics, Speech and Signal Processing (ICASSP)*, pages 8549–8553, 2020. 1
- [38] Hongyu Sun, Xining Cui, Yinjing Guo, and Anqing Ding. Simplified spike-timing dependent plasticity learning rule of spiking neural networks for unsupervised clustering. In *2019 IEEE 3rd Advanced Information Management, Communities, Electronic and Automation Control Conference (IM-CEC)*, pages 26–30, 2019. 1, 2
- [39] Ping Tak Peter Tang, Tsung-Han Lin, and Mike Davies. Sparse coding by spiking neural networks: Convergence theory and computational results, 2017. 2
- [40] Rodrigo C. Vergara, Sebastián Jaramillo-Riveri, Alejandro Luarte, Cristóbal Moëne-Loccoz, Rómulo Fuentes, Andrés Couve, and Pedro E. Maldonado. The energy homeostasis principle: Neuronal energy regulation drives local network dynamics generating behavior. *Frontiers in Computational Neuroscience*, 13:49, 2019. 4
- [41] Alex Vigneron and Jean Martinet. A critical survey of stdp in spiking neural networks for pattern recognition. In *2020 International Joint Conference on Neural Networks (IJCNN)*, pages 1–9, 2020. 1
- [42] Qinyi Wang, Yexin Zhang, Junsong Yuan, and Yilong Lu. Space-time event clouds for gesture recognition: From rgb cameras to event cameras. In *2019 IEEE Winter Conference on Applications of Computer Vision (WACV)*, pages 1826–1835, 2019. 8
- [43] B. Yin, F. Corradi, and S.M. Bohtë. Accurate and efficient time-domain classification with adaptive spiking recurrent neural networks. *Nat Mach Intell*, 3:905–913, 2021. 8
- [44] Aaron R. Young, Mark E. Dean, James S. Plank, and Garrett S. Rose. A review of spiking neuromorphic hardware communication systems. *IEEE Access*, 7:135606–135620, 2019. 1, 2
- [45] Tielin Zhang, Xiang Cheng, Shuncheng Jia, Mu ming Poo, Yi Zeng, and Bo Xu. Self-backpropagation of synaptic modifications elevates the efficiency of spiking and artificial neural networks. *Science Advances*, 7(43):eabh0146, 2021. 8